THE JOURNAL OF PHYSICAL CHEMISTRY B

Article

pubs.acs.org/JPCB

Anatomy of an Exciton: Vibrational Distortion and Exciton Coherence in H- and J-Aggregates

Roel Tempelaar,[†] Anna Stradomska,[†] Jasper Knoester,[†] and Frank C. Spano*[,‡]

[†]Zernike Institute for Advanced Materials, University of Groningen, Nijenborgh 4, 9747 AG Groningen, The Netherlands

[‡]Department of Chemistry, Temple University, Philadelphia, Pennsylvania 19122, United States

Supporting Information

ABSTRACT: In organic materials, coupling of electronic excitations to vibrational degrees of freedom results in polaronic excited states. Through numerical calculations, we demonstrate that the vibrational distortion field accompanying such a polaron scales as the product of the excitonic interaction field and the exciton coherence function. This scaling relation is derived analytically in the regime where excitonic interactions are weak, yet it is shown to remain valid for interaction strengths ranging up to physically relevant values. Moreover, it is not affected by the magnitude of exciton-vibrational coupling or the presence of disorder in the molecular transition energies, despite the dramatic changes observed in the excited state. An application to helical MOPV4 aggregates is presented, followed by a quantitative study of the vibrational distortion field when excitonic interactions are strong. Our findings allow for a straightforward interpretation of widely varying polaron profiles, thereby facilitating the characterization of organic excited states.

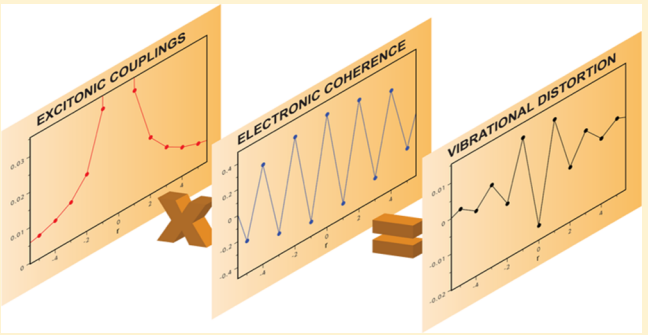

1. INTRODUCTION

The development of electronic devices based on organic semiconducting polymers and oligomers continues to receive a great deal of attention, driven by the promise of inexpensive and large-area solar cells, light-emitting diodes, and electronic paper, to name but a few applications. Organic materials offer a number of pivotal advantages over their inorganic counterparts, such as their chemical tunability and structural flexibility as well as the low cost and the ease with which they can be produced. However, these favorable features come at the expense of a strikingly complex organic solid state. A detailed understanding of the optical excitations in this solid state is a crucial step toward the next generation of organic electronics.

Characteristic of organic aggregates is the presence of exciton-vibrational (EV) coupling.[1−7] This coupling stems from organic systems being "soft", in the sense that electronic transitions are accompanied by a structural reorganization of the underlying molecular geometry. Hence, the aggregate acts as a dynamic grid through which charge and energy are transported. EV coupling, together with intermolecular excitonic interactions, leads to neutral polaronic excited states, consisting of a delocalized electronic excitation surrounded by vibrationally excited molecules, that is, by vibrational distortions. An additional factor affecting excitations in organic aggregates is disorder in the molecular transition energies, which severely limits the degree of delocalization.

The disordered Holstein model[1,2] provides a full quantum-mechanical treatment of energetic disorder, excitonic interactions, and linear EV coupling in calculating polaronic excited states. This model has proven to be successful in accurately describing the photophysics of a variety of organic molecular assemblies[8−15] and hence is considered to be a reliable framework in which detailed information about the excited states is easily accessible. To unravel the complicated nature of these states, several measures have been introduced, aimed to quantify the polaron characteristics. A familiar example is the spatial coherence function,[13,16] which measures the range over which the electronic excitation is coherently delocalized. Another frequently encountered measure is the vibrational distortion field[8,10,17] (VDF), quantifying the nuclear reorganization that accompanies the electronically excited state. The VDF is a very useful complement to the coherence function because it captures the structural flexibility that sets organic materials apart from those involved in conventional inorganic electronics.

The coherence function and the VDF seemingly relate to quite different aspects of the polaronic excited state. Nonetheless, we reveal a close connection between the two. In what follows, we show that the VDF $D^{em}(r)$ corresponding to the lowest-energy (emitting) exciton can be decomposed into the product of the coherence function $C^{em}(r)$ and the field of excitonic interactions $J(r)$ for small to intermediate excitonic couplings. This decomposition simplifies the characterization of polarons considerably and provides a deeper understanding of

Received: October 17, 2012
Revised: November 26, 2012

   dx.doi.org/10.1021/jp310298n | J. Phys. Chem. B XXXX, XXX, XXX−XXX

the mechanism underlying the polaronic state. Furthermore, it puts the VDF in a more familiar photophysical context.

This article is organized as follows. A brief review of the disordered Holstein model is given in Section 2, including a description of the coherence function and the VDF. This section concludes with the introduction of the aforementioned decomposition, scaling the VDF to the coherence function and excitonic interactions. A numerical demonstration of this relation is given in Section 3 for defect-free H- and J-aggregates. Localization of the emitting state due to defects or energetic disorder profoundly impacts the VDF, as is shown in Section 4. However, its scaling to the product of $J(r)$ and $C^{em}(r)$ is found to be maintained. Both for disordered and defect-free aggregates, the decomposition of the VDF can be derived analytically using excitonic coupling as a perturbation. The resulting expressions are presented in Sections 3 and 4; for more details, we refer to the Supporting Information. In Section 5, the applicability of our findings to organic molecular assemblies is discussed, using the helical aggregate MOPV4 as an example. This section continues with a brief study of nuclear reorganization in the regime of stronger excitonic interactions. Our conclusions are summarized and discussed in Section 6.

2. THEORY

A characteristic feature of organic molecular systems is the nonadiabatic coupling of the electronic excited states to vibrational degrees of freedom, such as stretching, bending, and breathing modes.[18,19] A notable example is the intramolecular symmetric ring-breathing/vinyl-stretching mode with a vibrational energy of ∼0.18 eV (∼1400 cm^{-1}), common to a variety of molecules with extended π-conjugation.[17,19,20] Vibrational modes are affected by electronic excitation, as the latter induces a structural reorganization of the molecules involved. A fully quantum mechanical treatment of this EV coupling is provided by the Holstein model,[1,2] in which the electronic excitation interacts linearly with one effective mode having a frequency ω_0. Expressed in units of the vibrational quantum $\hbar\omega_0$, and written in the basis of one-excitons, the corresponding Hamiltonian reads

$$H = \sum_n b_n^\dagger b_n + \lambda \sum_n (b_n^\dagger + b_n)|n\rangle\langle n| + \lambda^2 + \sum_{n,n+r} J(r)|n\rangle\langle n+r| + \sum_n \Delta_n|n\rangle\langle n| + \varepsilon_{0-0} \quad (1)$$

The vibrational energy is described by the first term, where $b_n^\dagger$ and b_n represent the bosonic ladder operators for the creation and annihilation of a vibrational quantum. EV coupling is accounted for by the second and third terms, through a shift of the minimum position of the harmonic vibrational potential upon electronic excitation by the amount of $-\lambda$. In what follows, the potential corresponding to the electronic excited state will be referred to as "shifted", whereas the ground-state potential is "unshifted". The square of the coupling constant, λ^2, is the Huang−Rhys factor,[18] which represents the nuclear reorganization energy following electronic excitation. The fourth term in eq 1 describes excitonic interaction between molecular sites n and $n+r$ through the coupling $J(r)$, where $|n\rangle$ denotes the purely electronic state in which molecule n is excited, whereas all other molecules reside in the ground state. The site-dependent deviation from the average 0−0 electronic transition energy ε_{0-0} is given by Δ_n, as is formulated by the last two terms in eq 1. This energetic disorder finds its origin in thermally induced deformations within molecular units (e.g. by twisting and bending) or randomness in the environment due to the presence of solvent molecules. The disorder values Δ_n are assumed to be static on the time scale of the relevant spectroscopic experiments.

As mentioned in the Introduction, the interplay of EV coupling and excitonic interactions results in the formation of polaronic Frenkel excitons (neutral polarons), which consist of a delocalized vibronic (both electronic and vibrational) excitation, surrounded by a "cloud" of purely vibrationally excited molecules.[19] An account for the coexistence of vibrons and vibrations is provided by the two-particle approximation.[9,21] Accordingly, the αth eigenstate of the disordered Holstein Hamiltonian is expanded as

$$|\Psi^\alpha\rangle = \sum_{n,\tilde{\nu}} c^\alpha_{n,\tilde{\nu}}|n, \tilde{\nu}\rangle + \sum_{n,\tilde{\nu}} \sum_{n',\nu'} c^\alpha_{n,\tilde{\nu};n',\nu'}|n, \tilde{\nu}; n', \nu'\rangle \quad (2)$$

Here the first term describes a delocalized vibronic excitation, with the single-particle state $|n,\tilde{\nu}\rangle$ representing an electronic excitation on molecule n involving $\tilde{\nu} \geq 0$ quanta in the shifted potential. For a two-particle state $|n,\tilde{\nu};n',\nu'\rangle$, such a vibron is accompanied by a vibration involving $\nu' \geq 1$ quanta in the unshifted potential of molecule n'. (Note that quanta in the shifted potential are denoted with a tilde to distinguish them from quanta in the unshifted potential.) The two-particle approximation drastically reduces the basis set in the Holstein model, whereas it is still found to accurately reproduce experimental spectra for a multitude of organic aggregates.[9,11−15,22] Typically, when the excitonic interactions exceed the vibrational quantum, the two-particle approximation should be extended to include three-particle terms as well (a vibron accompanied by two vibrationally excited molecules).[23,24] In the following, we use the two-particle approximation while limiting the total number of quanta, such that for all basis states $\tilde{\nu} + \nu' \leq \nu_{max}$. In all cases, convergence is assured with respect to ν_{max} as well as to three-particle terms.

The calculated wave function given by eq 2 can be used to characterize numerically the polaronic excited state. The first characteristic feature under consideration is the degree of coherent delocalization, quantified by the spatial coherence function[13,16]

$$C^\alpha(r) = \langle\Psi^\alpha| \sum_n B_n^\dagger B_{n+r}|\Psi^\alpha\rangle \quad (3)$$

Here $B_n^\dagger \equiv |n,\mathrm{vac}\rangle\langle g,\mathrm{vac}|$ is the local operator creating an electronic excitation at site n while leaving the vibrational wave function in the ground state of the unshifted potential (vacuum state). Note that $C^\alpha(r)$ is a straightforward extension of the electronic autocorrelation function to the case of nonzero vibronic coupling. As such, it embodies the profound difference between H- and J-aggregates. When the excitonic interactions are positive, as exists in H-aggregates, the coherence function of the band-bottom excited state changes phase as $(-1)^r$. The resulting wave function coefficients destructively contribute to the (principal) 0−0 optical transition strength, leading to a quenching of the corresponding emission peak.[25] For J-aggregates, with negative excitonic coupling, the band-bottom spatial coherence function has a uniform phase throughout, leading to constructive interference for the 0−0 peak, known as superradiance.[26]

dx.doi.org/10.1021/jp310298n | J. Phys. Chem. B XXXX, XXX, XXX−XXX

The nuclear reorganization that accompanies electronic excitations in organic aggregates is quantified by the VDF, given by[8,10,17]

$$D^{\alpha}(r) = \langle \Psi^{\alpha}| \sum_{n} |n\rangle\langle n| \frac{b_{n+r}^{\dagger} + b_{n+r}}{2} |\Psi^{\alpha}\rangle \tag{4}$$

The fraction appearing in the summand corresponds to the unitless vibrational coordinate operator. Hence, $D^{\alpha}(r)$ measures the average displacement from equilibrium of the vibrational potential pertaining to the molecular site that is r lattice spacings away from the electronic excitation. In other words, the VDF quantifies to what extent the polaron ranges *beyond* the delocalized electronic excitation.

The VDF has made a number of notable appearances in earlier studies. Scherer and Fischer used the distortion field as a means of checking the accuracy of a mean-field approach to polarons, with an application to aggregates of PIC molecules.[8] Later on, Hoffmann et al. utilized the VDF to characterize the band-bottom and band-top absorbing states in linear aggregates, specifically for PTCDA and MePTCDI.[10] In a similar fashion, this field was evaluated numerically for herringbone aggregates and for helical molecular assemblies in refs 17 and 13, respectively. In every case, the VDF was employed to provide a quantitative description of excitonic polarons, with relatively little attention given to the origin of, and the mechanisms involved in this characteristic field. Nonetheless, the occurrence of nonzero vibrational distortion for molecular sites other than the electronically excited one ($r = 0$) is both a relevant and an interesting phenomenon. It is relevant because noncentral ($r \neq 0$) distortion leads to an effective increase in the polaron's radius. The interesting part is that neighboring molecules, although not electronically excited, apparently experience a shift of the vibrational potential due to the presence of an adjacent exciton. Moreover, the VDF was occasionally found to predict such a potential shift to be directed oppositely to the distortion of the central vibron, thereby exhibiting very intricate behavior that was not completely understood.[13] This puzzling nature of the VDF will become much more comprehensible as we proceed.

We reveal an intimate relation between the VDF, the excitonic coupling field and the spatial coherence function. For the band-bottom polaronic state in a linear aggregate, a simple equation is found, scaling the noncentral distortion field to the product of the coherence function and the excitonic coupling field. Referring to the lowest-energy (emitting) eigenstate of the Holstein Hamiltonian as $\alpha = \mathrm{em}$, this equation reads

$$D^{\mathrm{em}}(r) = \Omega J(r) C^{\mathrm{em}}(r) \qquad (r \neq 0) \tag{5}$$

Here the prefactor Ω acts as a constant of proportionality that is determined by the Huang–Rhys factor λ^2 and the amount of energetic disorder but is independent of the intermolecular distance r. Furthermore, this scaling relation is not affected by the sign or the shape of the excitonic coupling field, allowing us to interpret a variety of polaron profiles, for both H- and J-aggregates. As will be demonstrated in the following sections, this scaling relation is formally valid when the excitonic interactions are small (as compared with the vibrational quantum). However, eq 5 turns out to accurately describe the VDF for physically relevant parameters, including excitonic interactions reaching the intermediate coupling regime.

3. HOMOGENEOUS AGGREGATES

In the absence of energetic disorder, the band-bottom electronic excitation is coherently delocalized over the entire aggregate, leading to a broad coherence function. Our findings, as formulated by eq 5, predict a corresponding VDF with a range similar to $J(r)$, which can be rather large for long range coupling.

Before proceeding, it is worthwhile to briefly elaborate on the formalism behind the VDF. In the absence of excitonic interactions, all excited states consist of localized vibrons. Consequently, such an excited molecule carries all of the vibrational distortion, as the VDF takes on the single-molecule value $D(r) = -\lambda\delta_{r,0}$. For increasing excitonic couplings, the vibrational distortion becomes distributed over neighboring molecules, giving rise to a nonzero noncentral VDF. All the way through, the bulk of the distortion is still found at $r = 0$. To conveniently study the effect of aggregation on the VDF, we will focus on the deviation from the single-molecule field, rather than the VDF itself. As such, the "VDF deviation" of the emitting exciton is defined as

$$\Delta D^{\mathrm{em}}(r) \equiv D^{\mathrm{em}}(r) + \lambda\delta_{r,0} \tag{6}$$

Furthermore, for weak to intermediate excitonic interactions, the total vibrational displacement, obtained by summing $D^{\mathrm{em}}(r)$ over all r, is found to be conserved and equal to $-\lambda$. (This conservation is exact when periodic boundary conditions are applied; see ref 20.) As a consequence, the total of the VDF deviation can be considered to equal zero. On the basis of these remarks, the scaling relation, as formulated in eq 5, can be recast in the more explicit form

$$\Delta D^{\mathrm{em}}(r) \approx \begin{cases} \Omega_{\mathrm{HOM}} J(r) C^{\mathrm{em}}(r) & (r \neq 0) \\ -\sum_{r' \neq 0} \Delta D^{\mathrm{em}}(r') & (r = 0) \end{cases} \tag{7}$$

As previously mentioned, the proportionality constant generally depends on energetic disorder. Its value in the homogeneous limit is indicated as Ω_{HOM}.

For homogeneous aggregates, the excited states are described using eq 1 while setting $\Delta_n = 0$ for all n. This Hamiltonian is diagonalized numerically in the basis of one- and two-particle states, see eq 2, to calculate the lowest-energy eigenstate $|\Psi^{\mathrm{em}}\rangle$. Substitution into eqs 3 and 4 then yields the corresponding spatial coherence function and VDF, respectively. Shown in Figure 1 are the results for a linear H-aggregate consisting of $N = 15$ molecules. The EV coupling strength is taken to be $\lambda^2 = 1$, which is a typical Huang–Rhys factor for organic materials.[17,19,20] Convergence is obtained for a vibrational truncation of $\nu_{\max} = 6$, a value that will be applied throughout. As depicted in Figure 1a, different distance-dependences of the excitonic interactions are used. The interactions scaling as $1/r^3$ (black circles) correspond to the well-known point-dipole couplings, which have been utilized as an approximation in many studies.[27−29] To investigate the effect of longer-ranged interactions, additional calculations are performed using $1/r^2$ (green triangles) and $1/r$ scaling (red squares). In all cases, the nearest-neighbor interaction $J(r = 1)$ is set to $10^{-3/2} \approx 0.032$ of the vibrational quantum. (The couplings are understood to depend on $|r|$, rather than on r. Hence, the scalings should formally be expressed in terms of absolute values, and for

dx.doi.org/10.1021/jp310298n | J. Phys. Chem. B XXXX, XXX, XXX−XXX

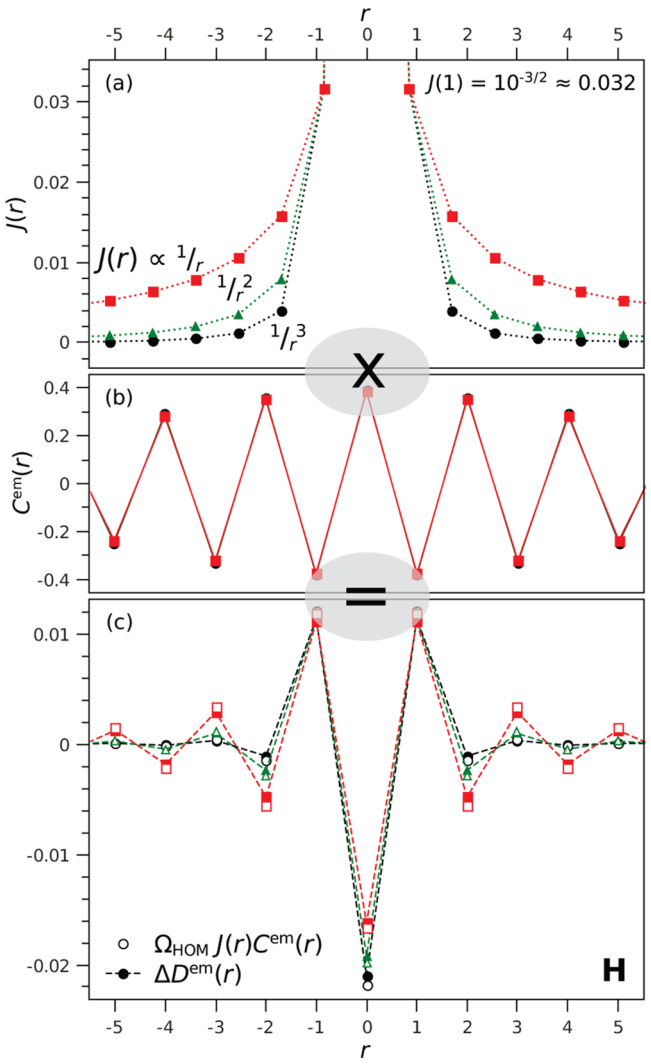

Figure 1. Numerically obtained characteristics for the emitting state of a disorder-free H-aggregate, consisting of $N = 15$ molecules with a Huang–Rhys factor of $\lambda^2 = 1$. As depicted in panel a, the excitonic interactions scale as $1/r$ (red squares), $1/r^2$ (green triangles), and $1/r^3$ (black circles), where r is the intermolecular separation. The nearest-neighbor coupling is fixed at $J(1) = 10^{-3/2}$ in units of $\hbar\omega_0$. The corresponding coherence functions almost completely overlap for all interaction scalings, as is shown in panel b. Panel c demonstrates the VDF deviation (solid symbols connected by dashed lines), together with the results of eq 7 (open symbols) with $\Omega_{HOM} = -1$. Accordingly, the open symbols represent the (negated) product of the excitonic couplings and coherence function when $r \neq 0$.

negative r, the couplings are of course obtained through $J(r) \equiv J(-r)$.)

Figure 1b displays the spatial coherence function, which turns out to be fairly insensitive to the range of the excitonic couplings. In any case, $C^{em}(r)$ exhibits phase oscillations, which in Section 2 was already referred to as a characteristic feature of the emitting state in H-aggregates. The function spreads over the entire aggregate but diminishes in amplitude with increasing $|r|$ due to end effects.

In Figure 1c, a comparison is made between the VDF deviation (solid symbols connected by dashed lines) and the right-hand side of eq 7, which will be referred to as the *JC* product. For all coupling ranges, the VDF deviation and *JC* product coincide almost completely, which allows us to account for the peculiar field conformation by means of the excitonic interactions and the spatial coherence function. First, the VDF deviation features a pronounced oscillation, which derives from the alternating sign of $C^{em}(r)$. This oscillation is damped with intermolecular distance r, in large part as a result of the envelope of $J(r)$. Note that the proportionality constant is negative. Its value for disorder-free aggregates with $\lambda^2 = 1$ is taken to be $\Omega_{HOM} = -1$, as will be justified later on. Upon extending the interactions range from $1/r^3$ to $1/r$, a strong increase is observed in the field magnitudes for $|r| \geq 2$. According to the *JC* product, this increase can be attributed entirely to the enhanced longer-range couplings because the coherence function remains almost unchanged. In contrast, the central VDF deviation *shrinks* as the coupling range increases, which according to eq 7 is due to a reinforced destructive interference in the summand for $r \neq 0$.

The fact that eq 7 holds equally well for J-aggregates is illustrated in Figure 2. Panel a repeats the H-aggregate results

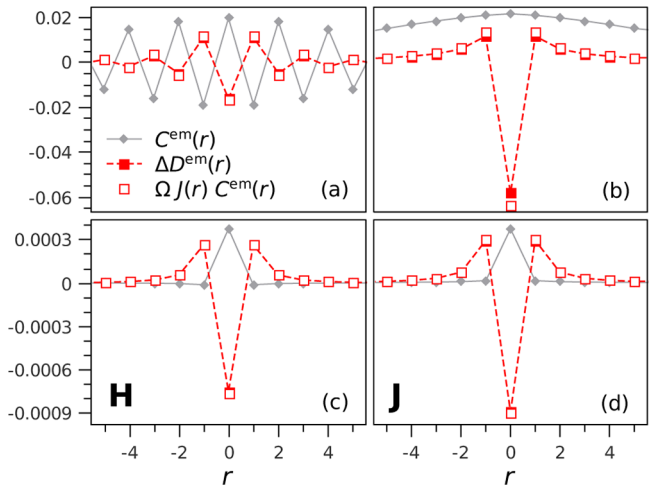

Figure 2. Calculated coherence function $C^{em}(r)$ (gray diamonds connected by solid lines), together with the VDF deviation (red solid squares connected by dashes) and the result of eq 7 (red open squares). The excitonic couplings, $J(r)$, scale as $1/r$, with $J(1) = 10^{-3/2}$ for H-aggregates (a,c) and $J(1) = -10^{-3/2}$ for J-aggregates (b,d). Results for the homogeneous limit are shown in panels a and b, using the prefactor $\Omega_{HOM} = -1$, whereas panels c and d present the outcome for the SIS model with $\Delta = 1$, using $\Omega_{SIS} = -0.65$. All other parameters are the same as in Figure 1.

from Figure 1 for couplings scaling as $1/r$. Here the gray diamonds connected by solid lines depict the coherence function, whereas the VDF deviation and the *JC* product are represented by red solid squares connected by dashes and red open squares, respectively. Panel b shows the numerical outcome for the same set of parameters, except for the excitonic interactions being negative. As briefly mentioned in Section 2, this corresponds to the case of a J-aggregate, for which the emitting state is uniform in phase. Indeed, the coherence function is monosignate this time, as is the resulting noncentral VDF deviation. Again, all of the VDF features can be accounted for by means of $J(r)$ and $C^{em}(r)$, as the scaling relation is satisfied remarkably well. Panels c and d will be discussed in Section 4.

Equation 7 is evaluated for different interaction strengths in Figure 3, which shows the VDF deviation (solid symbols connected by dashes) together with the *JC* product (open

dx.doi.org/10.1021/jp310298n | J. Phys. Chem. B XXXX, XXX, XXX–XXX

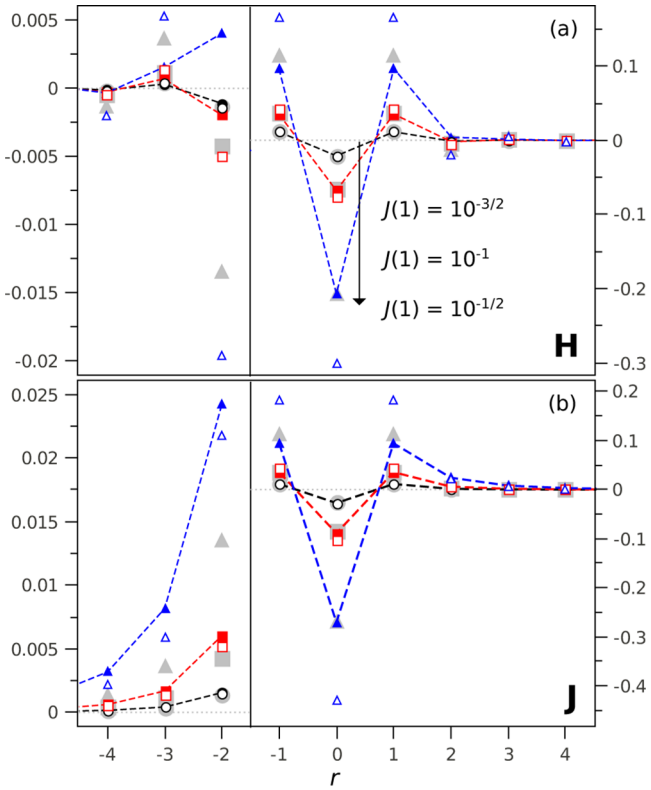

Figure 3. Calculated VDF deviation (solid symbols connected by dashes) together with the right-hand side of eq 7 (open symbols) for the case of point-dipole ($1/r^3$) interactions. Shown are the results for the nearest-neighbor coupling $J(1)$ having a magnitude of $10^{-3/2}$ (black circles), 10^{-1} (red squares), and $10^{-1/2}$ (blue triangles). All other parameters are the same as in Figure 1. Gray symbols indicate the outcome of eq 9. The results for H- and J-aggregates are presented in panels a and b, respectively. In both panels, the left frame shows a magnification of the fields for $r \leq -2$.

symbols) using varying magnitudes of point-dipole ($1/r^3$) interactions. Panel a demonstrates the results for an H-aggregate, whereas the case of a J-aggregate is depicted in panel b. All other parameters are identical to Figure 1, including $\Omega_{HOM} = -1$. For point-dipole couplings, the weight of the vibrational distortion is confined around the center. To appreciate the off-center distortion, both panels include a magnified portion of the field for $r \leq -2$. Our numerical results in Figure 3 show hints of $D^{em}(r)$ scaling to $J(r)$ times $C^{em}(r)$ being a weak-coupling relation, as the VDF deviation and the *JC* product start to diverge with increasing excitonic interactions. For $r = \pm 1$, this divergence increases to ~50% when the magnitude of $J(1)$ is increased to $10^{-1/2} \approx 0.32$ (blue triangles). In the case of an H-aggregate, a change of sign occurs at the higher field ends (demonstrated in the magnified panel on the left) that is not reproduced by the *JC* product because the exciton coherence function maintains its sign-alternating profile. As will be demonstrated in Section 5, these sign changes are early signatures of the regime of strong excitonic coupling, where the VDF levels off to a positive value that is constant for all r, indicative of a large-radius polaron. The VDF deviation of a J-aggregate was monosignate to begin with, and the absence of sign changes seems to allow the *JC* product to continue reproducing the VDF rather accurately for $|r| \geq 2$. In general, eq 7 appears capable of describing the overall VDF features for nearest-neighbor coupling as strong as $J(1) = 10^{-1}$ for both H- and J-aggregates.

The last part of this section is dedicated to a brief demonstration that eq 7 is indeed a weak-coupling result, as was already suggested above. Weak coupling here means that $J(r)$ is typically small when compared with the vibrational quantum, or in short notation $J \ll 1$.[30] In ref 31, this regime was employed to find the lowest-energy excited state of homogeneous aggregates by means of perturbation theory in the parameter J. Substitution of the resulting wave function into eq 3 yields an analytical expression for the spatial coherence function. (A detailed account is included in the Supporting Information.) Accordingly, the coherence function to zeroth order in the excitonic coupling is found to be[31]

$$C^{em}(r) = e^{-\lambda^2} \sum_n \phi_n^{em} \phi_{n+r}^{em} + O(J) \tag{8}$$

where the coefficients ϕ_n^{em} correspond to the lowest-energy eigenstate of the perturbation Hamiltonian $H^1 \equiv \sum_{n,n+r} J(r)\ |n\rangle\langle n+r|$ represented in the purely electronic basis. The exponential term derives from the vibrational overlap factor $f_{\tilde{\nu},\nu} \equiv \langle \tilde{\nu}|\nu\rangle$ between the harmonic oscillator eigenfunctions of $\tilde{\nu}$ quanta in the shifted potential and ν quanta in the unshifted potential. The special case of $\tilde{\nu} = 0$ and $\nu = 0$ relates to the Huang–Rhys factor through $f_{\tilde{0},0}^2 = e^{-\lambda^2}$.

In a similar fashion, an analytical equation for the VDF is found using eq 4. (Again, see the Supporting Information.) The noncentral VDF deviation to second order in J takes on the form

$$\Delta D^{em}(r \neq 0) = \Omega_{HOM} J(r) e^{-\lambda^2} \sum_n \phi_n^{em} \phi_{n+r}^{em} + O(J^2) \tag{9}$$

This expression, together with eq 8, identifies the noncentral VDF with the *JC* product, as formulated in the first line of eq 7. At the same time, the prefactor for the homogeneous limit is found to be the ratio of the $\tilde{0}$–1 to the $\tilde{0}$–0 overlap factor

$$\Omega_{HOM} \equiv -e^{\lambda^2} f_{\tilde{0},1} f_{\tilde{0},0} = -\frac{f_{\tilde{0},1}}{f_{\tilde{0},0}} \tag{10}$$

in units of $(\hbar\omega_0)^{-1}$. For $\lambda = 1$, these factors are equal, leading to the presumed relation $\Omega_{HOM} = -1$.

Besides confirming the scaling of the VDF deviation to the *JC* product, the foregoing analysis provided us with yet another expression for $\Delta D^{em}(r)$, relating this field to $J(r)$ and the pure-electronic wave function coefficients ϕ_n^{em}, see eq 9. This equation can be evaluated numerically without too much effort because it involves only a diagonalization of the electronic Hamiltonian H^1 instead of the full vibronic one. The resulting field values are presented in Figure 3 using gray symbols. In general, eq 9 reproduces the $r = \pm 1$ fields very accurately, lying within 10% of the VDF deviation for couplings as strong as $J(1) = 10^{-1/2}$. In the case of H-aggregates, it shows an improvement over the *JC* product throughout the entire field. This is possibly due to eq 9 being correct to second order in J, whereas the *JC* product is only correct to first order in J by virtue of eq 8. Surprisingly though, eq 9 performs worse than the *JC* product for the field ends of J-aggregates. Here we notice a sophisticated mechanism that intensifies with increasing J. Intriguing as it is, a detailed account is beyond the scope of our current work. In Section 5, we continue with a quantitative study for the regime of stronger couplings.

dx.doi.org/10.1021/jp310298n | J. Phys. Chem. B XXXX, XXX, XXX–XXX

4. EXCITON LOCALIZATION

The introduction of energetic disorder strongly impacts the spatial coherence of the emitting state, leading to localization of the exciton to the point where the state is substantially confined to the molecule with the lowest transition energy. Much like the coherence function, the extent of the VDF is also significantly affected. Nevertheless, the scaling of the VDF deviation to the *JC* product is not disturbed by exciton localization, and hence the corresponding collapses of $\Delta D^{em}(r)$ and $C^{em}(r)$ go hand-in-hand. This is shown in the current section by employing the single-impurity scattering (SIS) model. Introduced in ref 32, the SIS model mimics the effect of strong disorder by considering the lowest energy molecule as a detuned trap in an otherwise homogeneous aggregate. This simplification opens ways to derive analytically the scaling relation given by eq 5. As it turns out, detuning-induced localization affects only the prefactor Ω, leaving the general form of this relation unchanged.

The SIS model assumes molecule $\bar{n}$ to be energetically detuned by the amount of $-\Delta$ ($\Delta > 0$), whereas all other molecules are disorder-free. The corresponding Hamiltonian is given by eq 1 while setting

$$\Delta_n = -\Delta\delta_{n,\bar{n}} \tag{11}$$

The band-bottom eigenstate and the corresponding spatial coherence function and VDF deviation are calculated, through diagonalization in the basis of one- and two-particle states. By analogy to eq 9, the scaling relation is cast in the form

$$\Delta D^{em}(r) \approx \begin{cases} \Omega_{SIS}(\Delta) J(r) C^{em}(r) & (r \neq 0) \\ -\sum_{r' \neq 0} \Delta D^{em}(r') & (r = 0) \end{cases} \tag{12}$$

where the constant of proportionality is explicitly dependent on the trap depth Δ. The numerical evaluation of eq 12 is presented in Figure 2c and 2d for an H- and J-aggregate, respectively. To this end, a trap with a depth of $\Delta = 1$ is incorporated in a linear aggregate consisting of $N = 15$ molecules with a Huang–Rhys factor of $\lambda^2 = 1$. As will be verified later, this leads to a prefactor of $\Omega_{SIS}(\Delta = 1) = -0.65$. An average is taken over all possible impurity positions $\bar{n}$. The excitonic interactions $J(r)$ scale as $1/r$, with $J(1) = \pm 10^{-3/2}$. Also shown are the corresponding coherence functions.

In comparing the results for the SIS model with their homogeneous counterparts, recall Figure 2a,b, we observe a collapse of the spatial coherence (gray diamonds connected by solid lines). For both H- and J-aggregates, a trap depth equal to the vibrational quantum is sufficient for $C^{em}(r)$ to approach a delta peak at $r = 0$, whereas coherence is shared only slightly with neighboring molecules. Close inspection reveals that the noncentral coherence function is all negative for positive excitonic couplings in Figure 2c and visa versa in Figure 2d. As a consequence, the *JC* product predicts very similar distortion fields for the H- and J-aggregates. According to the calculated VDF deviations (red solid squares connected by dashes), this is indeed the case. Furthermore, the correspondence with the *JC* product (open squares) is excellent, confirming the validity of eq 12.

In the homogeneous limit, the scaling of $\Delta D^{em}(r)$ to the *JC* product proved to be a weak coupling relation. To investigate the dependence of eq 12 on the coupling strength, we have performed calculations for $J(1)$ ranging up to $10^{-1/2}$ of the vibrational quantum. The results for the case of an H-aggregate are demonstrated in Figure 4a, whereas panel b presents the outcome for J-aggregates. Beside $\Delta = 1$, all parameters are the same as those used in Figure 3, including excitonic interactions of the point-dipole type. The short range of these interactions in combination with the delta-like behavior of the coherence function predicts the field values to drop off with $|r|$ very rapidly so that all significant field intensity is carried by the nearest-neighbor values at $r = \pm 1$. As shown in Figure 4, these VDF values (solid symbols connected by dashes) are surprisingly well-reproduced by the *JC* product (open symbols), even for a nearest-neighbor coupling as strong as $J(1) = 10^{-1/2}$ (blue triangles). When compared with the homogeneous case, recall Figure 3, disorder-induced localization seems to improve rather than destroy the validity of the scaling relation. For H-aggregates, we again observe a sign mismatch for $|r| \geqslant 2$ (see inset). Most likely, the excitonic couplings become strong enough to induce "homogeneous" phase oscillations in the coherence function, whereas the VDF deviation remains monosignate. It is worth noting that the distortion field intensities in Figure 4 react severely to an increase in *J*. This turns out to be characteristic of disordered aggregates, as will become clear shortly.

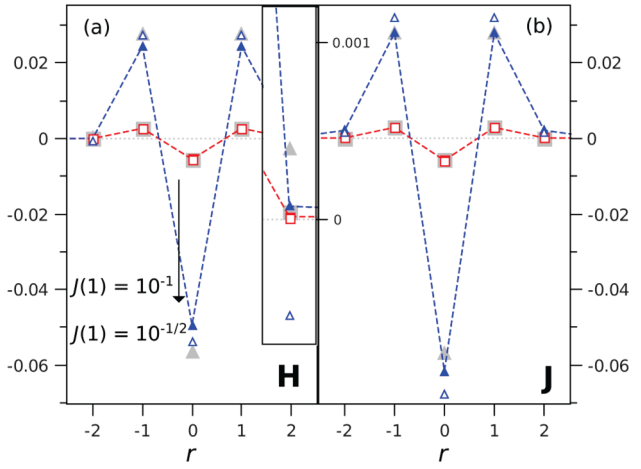

Figure 4. Numerical results for the single-impurity scattering model with a trap depth of $\Delta = 1$. Point-dipole ($1/r^3$) interactions are used while the nearest-neighbor coupling $J(1)$ is set to 10^{-1} (red squares) and $10^{-1/2}$ (blue triangles). The aggregate length is $N = 15$, whereas a Huang–Rhys factor of $\lambda^2 = 1$ is taken. Shown are calculated VDF deviations (solid symbols connected by dashes), together with the right-hand side of eq 12 (open symbols) using $\Omega_{SIS}(\Delta) = -0.65$. Also shown are the values predicted by eq 14 (gray symbols). Panel a demonstrates the results for an H-aggregate, where the inset shows the magnification of the $r = 2$ field values. The case of a J-aggregate is depicted in panel b.

The SIS model allows for an analytical verification of eq 12, similarly to what has been presented in Section 3 for the homogeneous case. This analysis is a straightforward extension of the formalism introduced in ref 32, where the band-bottom exciton was expressed as a perturbative expansion in *both* parameters *J* and J/Δ. Hence, this approach is valid in the weak-coupling regime, while further assuming a strong localization of the emitting exciton. The analytical extension, being straightforward yet elaborate, is outlined in the Supporting Information.

dx.doi.org/10.1021/jp310298n | J. Phys. Chem. B XXXX, XXX, XXX–XXX

What results is an expression for the exciton spatial coherence to first order in J/Δ

$$C^{\mathrm{em}}(r) = \mathrm{e}^{-\lambda^2}\left(\delta_{r,0} - 2J(r)\sum_{\tilde{\nu}\geq 0}\frac{f^2_{\tilde{\nu},0}}{\Delta + \tilde{\nu}}\right) + O(J^2) \tag{13}$$

Here higher-order corrections couple through *either* J/Δ or J, which is indicated by the simplified notation $O(J^2)$. The VDF deviation is of order J^2/Δ, taking on the form

$$\begin{aligned}\Delta D^{\mathrm{em}}(r \neq 0) &= J(r)^2 \sum_{\tilde{\nu},\nu'\geq 0} \Gamma_1(\Delta, \tilde{\nu}, \nu')(\Gamma_2(\tilde{\nu}, \nu') \\ &\quad + \sqrt{\nu' + 1}\,\Gamma_1(\Delta, \tilde{\nu}, \nu' + 1)) + O(J^3)\end{aligned} \tag{14}$$

Two new functions are introduced, both having units of $(\hbar\omega_0)^{-1}$. These are defined as

$$\Gamma_1(\Delta, \tilde{\nu}, \nu') \equiv -\frac{f_{\tilde{\nu},0} f_{\tilde{0},\nu'}}{\Delta + \tilde{\nu} + \nu'} \tag{15}$$

and

$$\Gamma_2(\tilde{\nu}, \nu') \equiv -f_{\tilde{\nu},1} f_{\tilde{0},\nu'} \tag{16}$$

The scaling of $\Delta D^{\mathrm{em}}(r)$ to the *JC* product, as formulated in eq 12, follows directly upon combining eqs 13 and 14. Meanwhile, the corresponding Δ-dependent constant of proportionality is found to have a rather complicated form

$$\begin{aligned}\Omega_{\mathrm{SIS}}(\Delta) = -\mathrm{e}^{\lambda^2}\Big(&\sum_{\tilde{\nu},\nu'\geq 0} \Gamma_1(\Delta, \tilde{\nu}, \nu')(\Gamma_2(\tilde{\nu}, \nu') \\ &+ \sqrt{\nu' + 1}\,\Gamma_1(\Delta, \tilde{\nu}, \nu' + 1))\Big)\Big/\left(2\sum_{\tilde{\nu}\geq 0}\frac{f^2_{\tilde{\nu},0}}{\Delta + \tilde{\nu}}\right)\end{aligned} \tag{17}$$

However, simple algebra reveals that this prefactor approaches the homogeneous value in the limit of vanishing trap depth

$$\lim_{\Delta\to 0} \Omega_{\mathrm{SIS}}(\Delta) = \Omega_{\mathrm{HOM}} \tag{18}$$

This is illustrated numerically in Figure 5, where $\Omega_{\mathrm{SIS}}(\Delta)$ is shown (solid symbols connected by lines) for different values of the detuning, with the Δ-independent Ω_{HOM} as an asymptote (open symbols connected by dashes). The Huang–Rhys factor is kept at $\lambda^2 = 1$. The Figure demonstrates good convergence of the detuned prefactor for $\Delta < 0.01$. Note that for $\Delta = 1$, Ω_{SIS} equals approximately -0.65; the value that was used in the numerical calculations presented in this section.

Accordingly, Ω_{HOM} manifests itself as a special case of the more general detuned prefactor. This implies that the analytical approaches in the homogeneous limit and in the SIS model, although being rather different, lead to exactly the same result in the limit of vanishing Δ. These findings indicate that the scaling of the VDF to the *JC* product is a general weak-coupling result that remains valid all the way through the transition from the coherent homogeneous regime ($\Delta = 0$) to the strongly incoherent SIS limit ($\Delta \gg J$). It is noteworthy that this transition is difficult to describe entirely by means of analytical methods. To verify the general weak-coupling validity of the scaling relation, we evaluate eq 5 numerically in Figure 6 while transiting from the homogeneous limit to a detuning of $\Delta = 1$, all the time using the detuned prefactor as given by eq 17. The

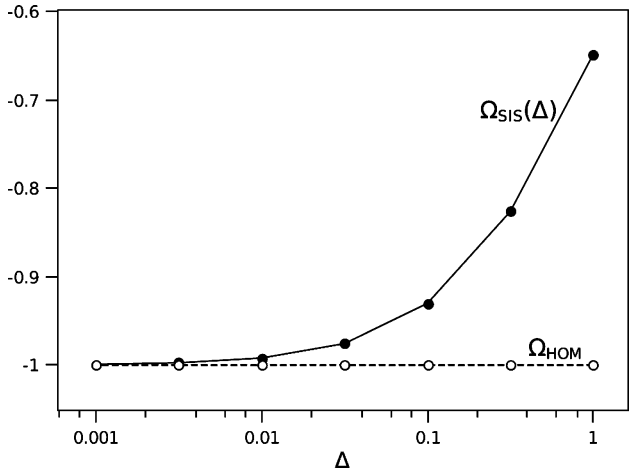

Figure 5. Calculated values of the prefactor $\Omega_{\mathrm{SIS}}(\Delta)$ corresponding to the SIS model, for a trap depth Δ varied by factors of $1/\sqrt{10}$. Shown as an asymptote is the Δ-independent homogeneous prefactor Ω_{HOM}. The Huang–Rhys factor is taken to be $\lambda^2 = 1$.

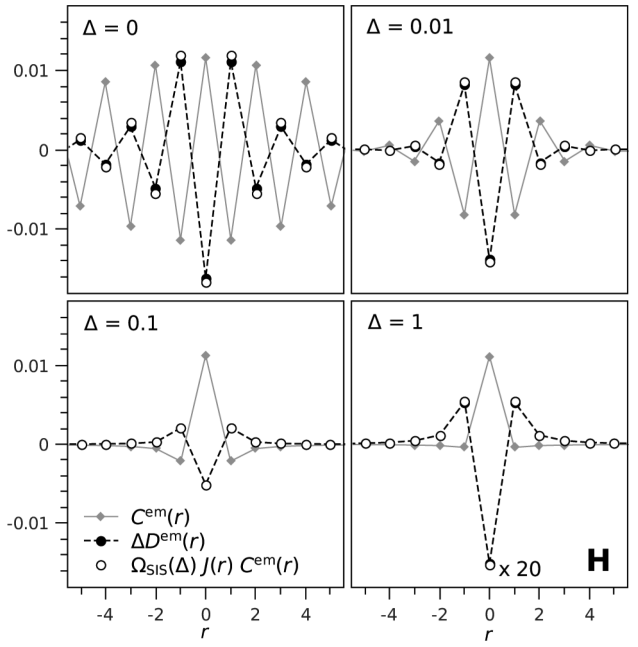

Figure 6. Field values for an H-aggregate detuned with different trap depths Δ. Gray solid diamonds connected by lines depict the coherence function. Also shown are the VDF deviation (black solid circles connected by dashes) and the right-hand side of eq 12 (open symbols). In both cases, the field values are magnified by a factor of 20 in the panel of $\Delta = 1$. The prefactor is taken from eq 17. Excitonic interactions scale as $1/r$ with a nearest-neighbor coupling of $J(1) = 10^{-3/2}$. The aggregate length is taken to be $N = 15$, and the Huang–Rhys factor is set to $\lambda^2 = 1$.

example of an H-aggregate is taken, using $1/r$ excitonic interactions. All other parameters are the same as in Figure 1. The coherence function (gray diamonds connected by solid lines) clearly reflects the gradual collapse that is expected when entering the disordered regime. Notice that the characteristic sign modulations disappear upon raising the trap depth from one percent to a tenth of the vibrational quantum. Throughout the entire transition, the *JC* product (black open circles) is found to agree nicely with the VDF deviation (black solid circles connected by dashes).

dx.doi.org/10.1021/jp310298n | J. Phys. Chem. B XXXX, XXX, XXX–XXX

The analytical confirmation of $\Delta D^{em}(r)$ scaling to the *JC* product in the SIS model has left us, again, with an alternative expression for the VDF deviation. Given by eq 14, this expression conveniently does not require any Hamiltonian diagonalization at all. It exhibits a quadratic scaling to J, which explains the drastic increase in the distortion field intensities upon enhancing the couplings, as previously observed in Figure 4. This Figure further confirms that eq 14, whose outcome is included using gray symbols, predicts equal field values for H- and J-aggregates, through its dependence on $J(r)^2$. The current analytical approach turns out to provide a nice complement of the *JC* product, as each method has its own pros and cons in reproducing $\Delta D^{em}(r)$ for increasing excitonic couplings. Note that eq 14 does resolve the sign mismatch for the fields at $r = \pm 2$. A further discussion of the (semi) analytical expression found for the SIS model, as well as for the homogeneous limit, is included in the Supporting Information.

5. APPLICATION TO MOPV4

When comparing the homogeneous limit to the single-impurity scattering (SIS) model, the introduction of an on-site trap appears to improve the scaling of the VDF to the product of excitonic interactions and the spatial coherence function. This is beneficial, of course, as most organic materials are inherently disordered. Nevertheless, it is difficult to pinpoint the regime of validity of eq 5 due to the complex interplay of disorder, excitonic interactions, and EV coupling. To exemplify the applicability of this scaling relation to actual molecular systems, the current section presents an examination of the helical aggregate MOPV4. This supramolecular assembly has received considerable attention lately[13,31−34] because it serves as an excellent model system for the study of organic optoelectronic materials. A few simplifications allow us to easily calculate the corresponding VDF and coherence function, providing qualitative insight into their interconnection for MOPV4 and alike molecular systems. (This is by no means intended as a quantitative study of the actual distortion field of MOPV4.) In the second part of this section, the regime of stronger couplings is investigated by artificially enhancing the MOPV4 excitonic interactions.

In MOPV4, the characteristic 1400 cm^{-1} vibrational mode couples to the (dominant) electronic transition with a strength of $\lambda^2 = 1.2$.[35] Helical aggregates of this chromophore can effectively be regarded as a linear chain of molecular units, for which the nearest neighbors experience a resonant excitonic coupling strength of 33 meV.[13] This corresponds to $J(1) = 0.2$ in units of the vibrational quantum $\hbar\omega_0 = 180$ meV. As such, MOPV4 is qualified in the intermediate coupling regime, for which $J \approx 1$. Overall, the excitonic interactions are predominantly positive, giving rise to H-aggregate behavior such as a quenching of the luminescence.[13] In MOPV4 helices, strong disorder confines the coherent range of the emitting exciton to only two to three molecules.[13] The absorption spectrum is appropriately reproduced by numerical simulations using a Gaussian distribution of site transition energies, incorporating a standard deviation of $\sigma = 85$ meV.[13] As shown in refs 14 and 36, the expected energy of the lowest-detuned molecule corresponds to 1.6σ below the average ε_{0-0} for an $N = 15$ aggregate length. We apply this value of N and utilize the SIS model with a detuning set equal to this expected trap depth, that is, $\Delta = 0.8$. The band-bottom excited state is calculated using the two-particle approximation, which has proven to be successful in describing the photophysics of MOPV4.[13] The excitonic interactions are taken from ref 13.

Figure 7 demonstrates the resulting VDF deviation (black solid symbols connected by dashes). Also shown is the *JC*

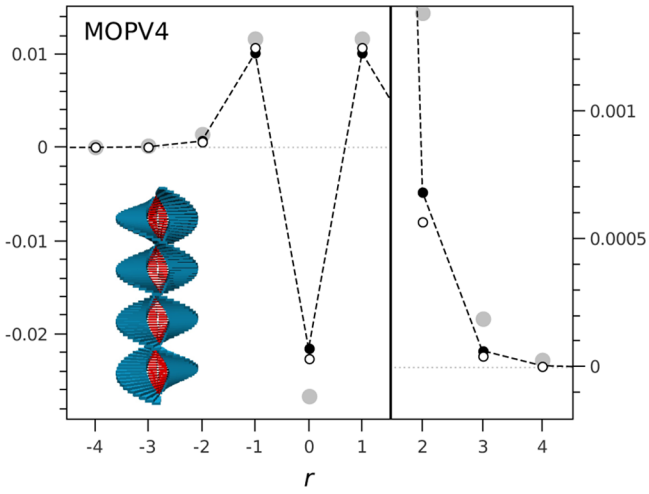

Figure 7. Numerical simulation of a helical MOPV4 aggregate using the SIS model with a trap depth of $\Delta = 0.8$. Excitonic couplings are taken from ref 13. Other parameters are $N = 15$ and $\lambda^2 = 1.2$. Demonstrated is the VDF deviation (solid symbols connected by dashes), together with the values predicted by eqs 12 (open symbols) and 14 (gray symbols). Right frame shows a detail of the fields for $r \geq 2$.

product (open symbols), with the prefactor calculated using eq 17. This product agrees with $\Delta D^{em}(r)$ to a large degree, providing the most accurate reproduction of the $|r| \geq 2$ field values we have seen for a magnitude of $J(1)$ this large. On the basis of these findings, the applicability of the scaling relation to actual molecular systems looks very promising. For completeness, Figure 7 additionally shows the analytically derived distortion field following eq 14 (gray symbols), which this time generates inferior results as compared with the *JC* product. It is worthwhile noting that generally the calculated field shows resemblance with the results for MOPV4 previously obtained in ref 13, for which a full distribution of (uncorrelated) disorder in the transition energies has been applied instead of the SIS model.

The VDF deviation was introduced in Section 3 to isolate the aggregation-induced contribution from the total of vibrational distortion, recall eq 6. In the remainder of this section, we return to the actual VDF and study its response to an increase in J, starting with the calculated MOPV4 interactions, denoted as J_{MOPV4}. In this regime of excitonic interactions, the contribution of local excitations accompanied by two purely vibrationally excited molecules starts to acquire significance, demanding the three-particle approximation to be applied.[23,24] The gain in accuracy comes at the cost of a rapidly increasing basis set, imposing severe restrictions on the aggregate length N and the vibrational truncation ν_{max}. Furthermore, convergence of this approximation with respect to four-particle terms is difficult to ensure because inclusion of these terms is prohibitively expensive. However, the marginal change we observed in the VDF upon extending the two-particle basis to include three-particle terms, indicates that the three-particle approximation is sufficient to describe the trends of the VDF. In what follows, the three-particle approximation is employed

dx.doi.org/10.1021/jp310298n | J. Phys. Chem. B XXXX, XXX, XXX−XXX

for an aggregate consisting of $N = 10$ molecules, while retaining $\nu_{max} = 6$. Figure 8 demonstrates results for different scalings of

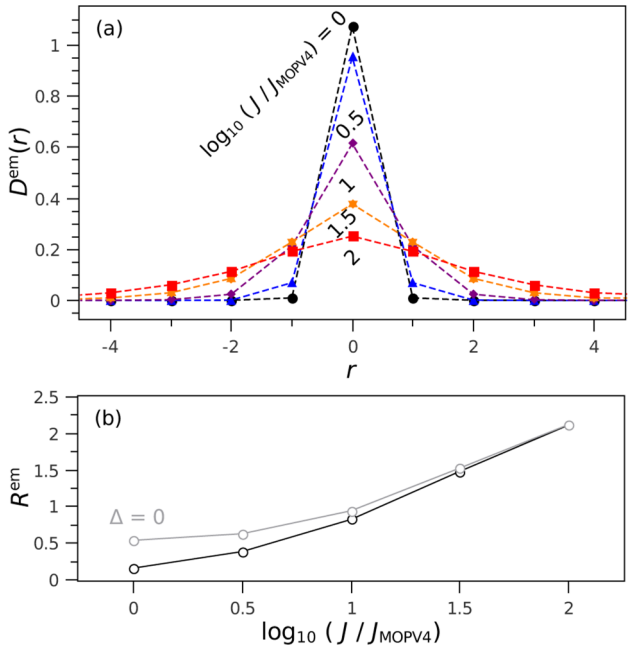

Figure 8. Numerical results for a linear aggregate consisting of $N = 10$ molecules. Excitonic interactions J are varied by scaling up the MOPV4 couplings J_{MOPV4}. All other parameters are the same as in Figure 7, including a trap depth of $\Delta = 0.8$. Shown in panel a is the VDF for $J/J_{MOPV4} = 1$ (black circles), $\sqrt{10}$ (blue triangles), 10 (purple diamonds), $10^{3/2}$ (yellow stars), and 100 (red squares). Panel b shows the polaron radius R^{em} versus the logarithm of the coupling strength for a detuned aggregate with $\Delta = 0.8$ (black curve) and for a homogeneous one with $\Delta = 0$ (gray curve).

J_{MOPV4}. Unscaled MOPV4 couplings are indicated using black circles and are essentially a repetition of the VDF shown in Figure 7. Subsequent multiplications with a factor $\sqrt{10}$ causes the distortion field to dramatically broaden. Upon a hundred-fold enhancement in J, a leveling-off is observable. This is a characteristic signature of the strong excitonic coupling regime, in which an excitation is coherently transferred to a neighboring molecule before significant vibrational relaxation can occur within the excited-state vibrational potential. By employing the Born−Oppenheimer approximation, it can be shown that in this limit the VDF approaches the value $-\lambda/N$ for all r, creating a large-radius polaron.[37] This coupling regime is interesting to study using a delocalized basis set.

As a sensible measure to quantify the enhancement in delocalized vibrational distortion with increasing J, we introduce the "polaron radius" as the unnormalized standard deviation of the VDF spatial extent. As such, the VDF is considered to be a symmetric distribution over the intermolecular distance r. Accordingly, the polaron radius is given by

$$R^{em} \equiv \left(\sum_r r^2 |D^{em}(r)|\right)^{1/2} \tag{19}$$

where the absolute value of $D^{em}(r)$ is applied to correct for possible negative distortions. Shown in Figure 8b is the polaron radius (black curve) as a function of the MOPV4 coupling scale for the distortion fields presented in panel a. As follows from the Figure, R^{em} nicely reflects the enhancements in the VDF, starting at a value of ∼0.2 for (unscaled) MOPV4, while steadily growing with J. Also shown are results obtained without applying the detuning (gray curve). When compared with these homogeneous results, R^{em} for detuned aggregates initially is suppressed by the disorder-induced collapse of the VDF. However, the scaling to J^2 allows the detuned radius to catch up with the homogeneous one, which scales linearly to the couplings strength, compare eqs 9 and 14. The difference in radii vanishes around $J = 100J_{MOPV4}$, where the effect of the impurity is overpowered by the strong excitonic interactions. Meanwhile the polaron radius grows to ∼2. A further increase in J will ultimately result in convergence of R^{em} toward a limiting N-dependent value.

6. CONCLUSIONS AND DISCUSSION

In organic materials, various factors act in concert to create excited states of a complex nature. Intermolecular excitonic interactions result in a delocalization of the exciton, which is offset by the localizing effects of EV coupling and inhomogeneities in the molecular transition energies (disorder). Furthermore, the combination of EV coupling and excitonic interactions leads to polaronic states, in which delocalized electronic excitations are accompanied by a significant distortion field distributed over the surrounding molecular nuclei. In this work, we have revealed an intimate connection between this VDF and the spatial coherence of the exciton, which helps to unravel the polaron's anatomy.

For the lowest-energy (emitting) state in linear aggregates, the vibrational distortion field surrounding the vibronically excited molecule, $D^{em}(r)$, is simply equal to the product of the exciton coupling field $J(r)$, the coherence function $C^{em}(r)$, and an r-independent prefactor Ω; see eq 5. The decomposition is exact in the limit of weak excitonic coupling and applies only to noncentral values of r ($r \neq 0$). The presence of disorder solely affects the prefactor Ω, leaving the scaling relation essentially unchanged. Moreover, eq 5 is independent of the range and sign of the excitonic interactions and hence is applicable to a diversity of H- and J-aggregates. The only restriction is that the interactions are small as compared with the vibrational quantum because eq 5 is a weak-coupling outcome, although rather accurate results are obtained for the intermediate coupling regime as well.

The validity of eq 5 is demonstrated through numerical simulations of disorder-free H- and J-aggregates in Section 3, for which the exciton coherence ranges over all participating molecules. Calculations in Section 4 indicate that the scaling relation remains valid even when the emitting state is localized, and the coherence function practically collapses to a delta function centered at the vibronic excitation. Exciton localization is realized by lowering the transition energy of a single molecule by the amount of Δ, which is referred to as the SIS model. The trap depth Δ solely impacts the prefactor Ω, leaving the scaling of the VDF to $J(r)$ and $C^{em}(r)$ unperturbed.

In Section 6, the scaling relation is evaluated for helical MOPV4 aggregates while utilizing the SIS model as a simplified representation. Primarily intended to examine the applicability of eq 5 in describing the typical distortion fields of organic materials, the resulting product of $J(r)$ and $C^{em}(r)$ does reproduce the VDF extremely well. The effect of stronger excitonic couplings on the VDF is analyzed in the remainder of this section through numerical simulations for enhanced MOPV4 interactions. Although being significantly localized at $r = 0$ for weak couplings, $D^{em}(r)$ gradually spreads out over the

dx.doi.org/10.1021/jp310298n | J. Phys. Chem. B XXXX, XXX, XXX−XXX

entire aggregate. This is reflected in the polaron radius, which is defined as the standard deviation of the VDF spatial extent.

An ongoing topic of interest is the connection between polaron characteristics and experimental observables. Recently, the spatial coherence function was shown to be reflected in the emission spectrum,[12−14] for which the 0−0 optical transition can be expressed as the sum $\sum_r C^{em}(r)$. In the case of helical aggregates, information on exciton coherence is contained in the circularly polarized luminescence spectrum as well.[23,31] Other studies have related details of excitonic couplings to circular dichroism[38] and circularly polarized luminescence.[32] In contrast, no such spectroscopic association was known for the VDF, rendering this exciton property merely a theoretical construct. However, its scaling to $C^{em}(r)$ and $J(r)$ contributes significantly to bridging this gap between the VDF and experiments.

Our study has focused on the VDF of completely delocalized emitting excitons as well as excitons localized by a single trap. In a future work, we will verify that the VDF in linear aggregates with distributed disorder can also be decomposed into the product of $J(r)$ and $C^{em}(r)$, with a special focus on the role of spatial correlation in the molecular transition energies.[13,38] Finally, we will explore the validity of eq 5 in multidimensional conformations such as sheets and films. This would have intriguing implications for systems including both positive and negative excitonic interactions.[17]

The anatomy of the polaron significantly impacts transport properties and hence plays an important role in the performance of organic-based electronic devices. Although the polaron radius can probably be addressed as being the most influential feature, other details of the VDF, such as the presence or absence of phase oscillations, may also be important and will be the subject of future studies. A growing understanding might lead to novel design strategies which exploit the dynamic nuclear framework to enhance the performance of organic electronic devices.

■ ASSOCIATED CONTENT

Supporting Information

Analytical derivations of spatial coherence function and vibrational distortion field in the homogeneous limit and in the SIS model. This material is available free of charge via the Internet at http://pubs.acs.org/.

■ AUTHOR INFORMATION

Corresponding Author

*E-mail: spano@temple.edu.

Notes

The authors declare no competing financial interest.

■ ACKNOWLEDGMENTS

A.S. acknowledges The Netherlands Organization for Scientific Research for support through a VENI grant. F.C.S is supported by the National Science Foundation, grant no. DMR-1203811.

■ REFERENCES

(1) Holstein, T. *Ann. Phys.* **1959**, *8*, 325−342.
(2) Holstein, T. *Ann. Phys.* **1959**, *8*, 343−389.
(3) Toyozawa, Y. *Prog. Theor. Phys.* **1961**, *26*, 29−44.
(4) Grover, M. K.; Silbey, R. *J. Chem. Phys.* **1970**, *52*, 2099−2108.
(5) Davydov, A. S. *Theory of Molecular Excitons*; Plenum: New York, 1971.
(6) Levinson, Y. B.; Rashba, E. I. *Rep. Prog. Phys.* **1973**, *36*, 1499−1565.
(7) Agranovich, V. M. *Excitations in Organic Solids*; Oxford University Press: New York, 2009.
(8) Scherer, P. O. J.; Fischer, S. F. *Chem. Phys.* **1984**, *86*, 269−283.
(9) Spano, F. C. *J. Chem. Phys.* **2002**, *116*, 5877−5891.
(10) Hoffmann, M.; Soos, Z. G. *Phys. Rev. B* **2002**, *66* (024305), 1−18.
(11) Lim, S.-H.; Bjorklund, T. G.; Spano, F. C.; Bardeen, C. J. *Phys. Rev. Lett.* **2004**, *92* (107402), 1−4.
(12) Spano, F. C. *J. Chem. Phys.* **2005**, *122* (234701), 1−15.
(13) Spano, F. C.; Meskers, S. C. J.; Hennebicq, E.; Beljonne, D. *J. Am. Chem. Soc.* **2007**, *129*, 7044−7054.
(14) Spano, F. C.; Clark, J.; Silva, C.; Friend, R. H. *J. Chem. Phys.* **2009**, *130* (074904), 1−16.
(15) Spano, F. C. *J. Am. Chem. Soc.* **2009**, *131*, 4267−4278.
(16) Chachisvilis, M.; Kühn, O.; Pullerits, T.; Sundström, V. *J. Phys. Chem. B* **1997**, *101*, 7275−7283.
(17) Spano, F. C. *J. Chem. Phys.* **2003**, *118*, 981−994.
(18) Huang, K.; Rhys, A. *Proc. R. Soc. London, Ser. A* **1950**, *204*, 406−423.
(19) Spano, F. C. *Acc. Chem. Res.* **2009**, *43*, 429−439.
(20) Hennessy, M. H.; Pascal, R. A., Jr.; Soos, Z. G. *Mol. Cryst. Liq. Cryst.* **2001**, *355*, 41−63.
(21) Philpott, M. R. *J. Chem. Phys.* **1971**, *55*, 2039−2054.
(22) Stradomska, A.; Petelenz, P. *J. Chem. Phys.* **2009**, *130* (094705), 1−9.
(23) Spano, F. C.; Zhao, Z.; Meskers, S. C. J. *J. Chem. Phys.* **2004**, *120*, 10594−10604.
(24) Stradomska, A.; Petelenz, P. *J. Chem. Phys.* **2009**, *131* (044507), 1−8.
(25) Oelkrug, D.; Egelhaaf, H.-J.; Gierschner, J.; Tompert, A. *Synth. Met.* **1996**, *76*, 249−253.
(26) Fidder, H.; Knoester, J.; Wiersma, D. A. *Chem. Phys. Lett.* **1990**, *171*, 529−536.
(27) Fidder, H.; Knoester, J.; Wiersma, D. A. *J. Chem. Phys.* **1991**, *95*, 7880−7890.
(28) Malyshev, V.; Moreno, P. *Phys. Rev. B* **1995**, *51*, 14587−14593.
(29) Didraga, C.; Knoester, J. *J. Lumin.* **2004**, *110*, 239−245.
(30) Note that this is a rather strict application of weak-coupling criteria, as outlined in: McRae, E. G.; Siebrand, W. *J. Chem. Phys.* **1964**, *41*, 905−906.
(31) Spano, F. C.; Meskers, S. C. J.; Hennebicq, E.; Beljonne, D. *J. Chem. Phys.* **2008**, *129* (024704), 1−14.
(32) Tempelaar, R.; Stradomska, A.; Knoester, J.; Spano, F. C. *J. Phys. Chem. B* **2011**, *115*, 10592−10603.
(33) Schenning, A. P. H. J.; Jonkheijm, P.; Peeters, E.; Meijer, E. W. *J. Am. Chem. Soc.* **2001**, *123*, 409−416.
(34) Korevaar, P. A.; George, S. J.; Markvoort, A. J.; Smulders, M. M. J.; Hilbers, P. A. J.; Schenning, A. P. H. J.; de Greef, T. F. A.; Meijer, E. W. *Nature* **2012**, *481*, 492−496.
(35) Cornil, J.; Beljonne, D.; Heller, C. M.; Campbell, I. H.; Laurich, B. K.; Smith, D. L.; Bradley, D. D. C.; Mullen, K.; Brédas, J. L. *Chem. Phys. Lett.* **1997**, *278*, 139−145.
(36) van Dijk, L.; Bobbert, P. A.; Spano, F. C. *J. Phys. Chem. B* **2009**, *113*, 9708−9717.
(37) Note that in the strong excitonic coupling regime, provided that periodic boundary conditions are applied, the VDF and the coherence function are related through $D(r) = -\lambda e^{\lambda^2} x^r C(r)$, with $x = 1$ and -1 for J- and H-aggregates, respectively.
(38) van Dijk, L.; Bobbert, P. A.; Spano, F. C. *J. Phys. Chem. B* **2010**, *114*, 817−825.